Nano Energy 73 (2020) 104764

Contents lists available at ScienceDirect

Nano Energy

journal homepage: http://www.elsevier.com/locate/nanoen

Flexible sliding sensor for simultaneous monitoring deformation and displacement on a robotic hand/arm

Zuqing Yuan [a,b,c,d], Guozhen Shen [e,f,**], Caofeng Pan [a,b,c,*], Zhong Lin Wang [a,c,g,***]

[a] CAS Center for Excellence in Nanoscience, Beijing Key Laboratory of Micro-nano Energy and Sensor, Beijing Institute of Nanoenergy and Nanosystems, Chinese Academy of Sciences, Beijing, 100083, China
[b] College of Physics and Optoelectronic Engineering, Shenzhen University, Shenzhen, 518060, China
[c] School of Nanoscience and Technology, University of Chinese Academy of Sciences, Beijing, 100049, China
[d] Institute of Microscale Optoelectronics, Shenzhen University, Shenzhen, 518060, China
[e] State Key Laboratory for Superlattices and Microstructures, Institute of Semiconductors, Chinese Academy of Sciences, Beijing, 100083, China
[f] Center of Materials Science and Optoelectronics Engineering, University of Chinese Academy of Sciences, Beijing, 100049, China
[g] School of Materials Science and Engineering, Georgia Institute of Technology, Atlanta, GA, 30332-0245, USA

ARTICLE INFO

Keywords:
Flexible electronics
Sliding sensor
Triboelectric nanogenerator
Capacitive sensor
Robotic application

ABSTRACT

Clamping manipulators known as end effectors, are applied to achieve the gripping function of objects basically and to overcome the inconvenience and hard work for human hands. Among them, the development of flexible manipulators has received wide attention. However, the existing gripper processes confine the gripping manner, and grasped objects may slide due to the insufficient friction force. Here, we demonstrate a multifunctional and integrated sliding sensor to provide a flexible sensing scheme for soft robotic manipulators to achieve high sensitivity and intelligent recognition. The sensing device combines a capacitive sensor with a triboelectric nanogenerator (TENG) based sensor, to provide possible approaches to control gripping and avoid unexpected slipping and damage, during the flexible gripping process.

1. Introduction

Clamping manipulators known as end effectors, are applied to achieve the gripping function of objects basically, regardless of the transfer robot or the assembly robot [1,2]. The mechanical graspers usually appear in the specialized cases, to overcome the inconvenience and hard work for human hands [3]. Nowadays, conventional hand portion of three- or four-finger deformable fingers with purely mechanical structure, present a similar design for shape and leaves a problem of slow crawling and narrow adaptability [4]. These conventional graspers made of rigid materials have a degree of difficulty to control and grasp the diverse shapes, sizes, irregularly-placed objects, especially for the holding stability.

Subsequently, the development of flexible clamping manipulators has received wide attention [5–9]. For example, air-suction-type end effector grip large, fragile or soft workpieces, with easy on-off control from the air source, and process more stable gripping. This gripping robotic hand is more adaptable to meet a wide range of the end effector [10]. However, the existing gripper processes confine gripping manner, and it bears large, frequent deformation and is difficult to grasp sheet-like objects. Meanwhile, the gripper is required to generate sufficient force to grip the object, grasped objects may slip due to the insufficient friction force when gripping flat-panel, smooth-surface objects. Accordingly, it is desirable to have a technical solution to overcome or at least mitigate at least one of the above drawbacks.

Integrated sensors that can obtain information such as the magnitude and location of a gripping force and whether an object slides may be a smart solution for robotic graspers, which control the operation and mechanical output [11–14]. Various sensors have been developed to detect changes from the surroundings [15–17] and to transfer physical

* Corresponding author. CAS Center for Excellence in Nanoscience, Beijing Key Laboratory of Micro-nano Energy and Sensor, Beijing Institute of Nanoenergy and Nanosystems, Chinese Academy of Sciences, Beijing, 100083, China.
** Corresponding author. State Key Laboratory for Superlattices and Microstructures, Institute of Semiconductors, Chinese Academy of Sciences, Beijing, 100083, China.
*** Corresponding author. CAS Center for Excellence in Nanoscience, Beijing Key Laboratory of Micro-nano Energy and Sensor, Beijing Institute of Nanoenergy and Nanosystems, Chinese Academy of Sciences, Beijing, 100083, China.
E-mail addresses: gzshen@semi.ac.cn (G. Shen), cfpan@binn.cas.cn (C. Pan), zhong.wang@mse.gatech.edu (Z.L. Wang).

https://doi.org/10.1016/j.nanoen.2020.104764
Received 25 February 2020; Received in revised form 25 March 2020; Accepted 28 March 2020
Available online 6 April 2020

information into electrical or optical signals that can be directly used by machines and humans [18–21]. To detect the degree of sliding between a robot arm and a gripping object, sliding sensors mainly monitor the shearing force and the relative displacement [22,23]. Currently, sliding sensors have large physical size, weight and complicated wiring, thus making them inconvenient to ensure detection accuracy and flexibility at the same time.

The design in this paper is for a multifunctional and integrated sliding sensor to provide a flexible sensing scheme for the soft robotic manipulators to achieve high sensitivity and intelligent recognition. The proposed design combines a high-sensitivity capacitive sensor [24,25] with a triboelectric nanogenerator (TENG) based sensor [26–29]. TENG is based on the coupling effect of contact electrification and electrostatic induction. When two different materials are in contact with each other under external force, their surfaces will generate equal amounts of positive and negative electrostatic charges due to contact electrification. And when the separation occurs in space, the induced potential difference is generated in the back electrodes, and the electrons are driven to flow in the external circuit to realize the supply of electrical energy. Therefore, TENGs can be used as a self-powered sensor for mechanical force, with multifunctional and active characteristics, which have potential applications in touch screens and electronic skins [30–32]. The capacitive sensor recognizes compressive stress and deformation, while the TENG provides a means for identifying the displacement and velocity of the contact object. The combination of the two parts can achieve a rich collection of physical changes through the electrical signals, to provide possible approaches to control gripping and avoid unexpected slipping and damage, during the flexible gripping process.

2. Experimental section

2.1. Device fabrication process

A copper conductive tape with a width of 5 mm is attached along the midline of a PET or some other substrate, and leaves extra space for encapsulation around. Then the connecting wire is added and the whole structure is covered by PU film. Another copper tape is stuck along the midline of PI tape. After introducing a lead wire, the copper tape is aligned and placed on the former one which is separated by the PU film. Then the entire part is sealed with a small air gap left between the PI and PU films. Based on the previously fabricated capacitive part, copper tape is attached to the outer surface of the PI film and aligned. The entire surface is then covered with an FEP film. Finally, the entire device is tailored to a slim shape with a width of 10 mm. The entire thickness was less than 0.2 mm. The PI and PU were viscous at the back. As for the device attached on the epidermis, the device is fabricated in reverse sequence and stuck directly onto the skin without the PET substrate.

2.2. Pressure measurement

Steel weights are placed on a hard-acrylic substrate (side length of 2 mm) as the load that presses the sensor from the triboelectric part. As the weight gradually increases, and corresponding capacitance is recorded by the LCR meter (E4980AL, Keysight). The measurement parameters are set with a frequency of 300 kHz and an alternating voltage of 1 V.

2.3. Deformation measurement

The device is kept horizontally with two ends fixed at the linear motor and the three-dimensional stage. Before the test, the device is aligned to keep the device straight. The distance between the two ends is then gradually reduced by the linear motor, and the device begins to deform. The corresponding capacitance is also recorded by the LCR meter. And for each small step, the capacitance is recorded for 5 s.

2.4. Sliding measurement setting up

The flexible sliding sensor is flatly attached to the optical horizontal lifting platform, and foam tape is used on the back of the device to ensure soft contact with the sample. The tested device is chosen with an effective length of 8 cm, and the electrode wire is connected from one end to an electrometer (Keithley 6514). A data acquisition card (NI PXI-6259) is used to collect data in real-time. An A4 paper sample (width of 10 mm) has adhered to a hard acrylic plate. The acrylic plate is adhered to the linear motor to keep the A4 paper outwards to contact the FEP film when the linear motor pushes the acrylic plate back and forth. The A4 paper is softly pressed on the sliding sensor to reduce frictional losses.

For testing the relationship between displacement and signals, the linear motor pushes the sample forward with a fixed sliding speed of 0.1 ms^{-1}. During the process, the corresponding open-circuit voltage and transferred charges are monitored. The sliding displacement started at 10 mm, with a 5 mm increment for each test and 1 s of rest time before stopping at the end. While for testing the relationship between velocity and signals, the displacement is fixed with 30 mm.

3. Results and discussion

The flexible sliding sensor is designed as a thin-film device, which is divided into two functional parts from top to bottom, shown in Fig. 1a. The detailed fabrication process is shown in the experimental section. The outer part works as TENG to sense the contact sliding, which results from the Maxwell displacement current [33,34]. The inner part is a capacitive sensor to detect the compressive pressure, which encapsulates an air gap between the polyimide (PI) and polyurethane (PU) films to improve the sensitivity to pressure. Based on the above design, the entire structure is light, compact, and easy to bend, and thin to attach to an irregular surface, as shown in Fig. 1b.

Cross-section of the sensor is shown in Fig. S1 and the divided functions are illustrated in Fig. 1c and d. The FEP film is a typical negatively triboelectric material that gains electrons on the surface when in contact with an external object [35]. Accordingly, the contact object is positively charged with the same amount of opposite charges on the FEP surface. The output of sensing sliding motion is induced by relative displacement between the charged surfaces. When an object slides on the surface, opposite charges are induced in the copper electrode on the back of the fluorinated ethylene propylene (FEP) film. The sliding motion generates a small potential difference along the long electrode to the ground end, resulting in an amount of charge transferring between the electrode and the ground, shown in Fig. 1c. As for the capacitive sensor, a small dielectric spacer made of an air gap and PU film is between the two Cu electrodes, while all around is sealed tightly. When an external force presses on the device, the dielectric spacer is compressed, which results in a larger capacitance of the device [36]. So, the capacitive sensor can identify both compressive stress and deformation of the entire device that brings in strains in the dielectric spacer, which is shown in Fig. 1d.

To verify the sensitivity of the capacitive sensor, a flexible sliding sensor with an effective sensing area of 2×1 cm^2 is fabricated to test the pressure. Acrylic plate is used to apply pressure and extra load weight is put on the above surface. The curve of capacitance changes to pressure is shown in Fig. 2a. The results show that the sensitivity is higher below 1 kPa, which is 0.720 kPa^{-1}, while gradually saturated for larger pressure. Additionally, two different kinds of a dielectric spacer, whether there is a microstructure on the PU surface, were compared on the performance of the capacitive sensor (Fig. S2).

Uniformity experiment is carried out along the length of the device. A flexible sliding sensor with an 8 cm effective length was placed flatly on the table and then pressed by four fingers from left to right. The effective length means the length of overlapping electrodes in an effective functional area, which can be also explained that the length of

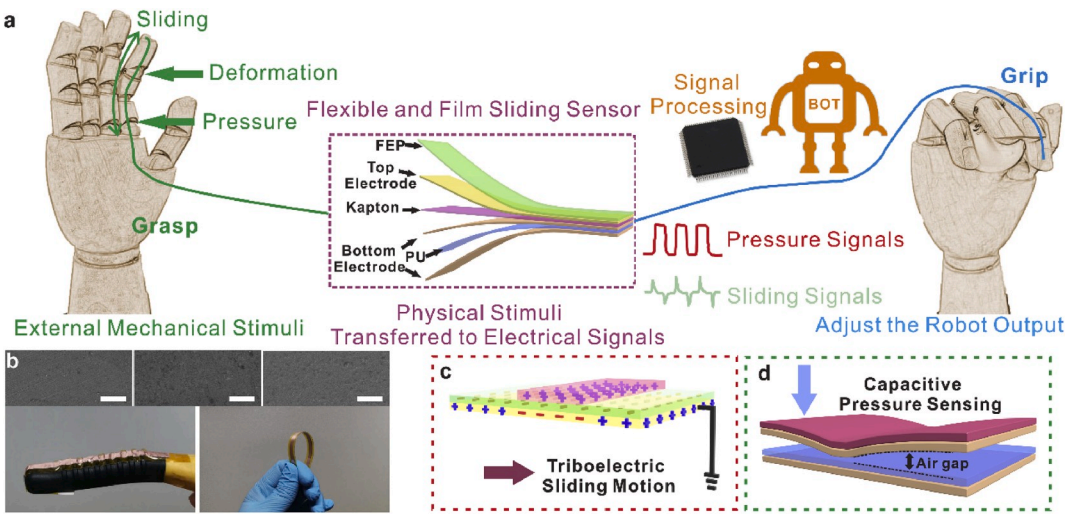

Fig. 1. Schematic structure and working principle of the flexible sliding sensor. (a) Schematic diagram of the flexible sliding sensor. This device can be used to attach on the finger surface to sense the pressure and sliding signals. (b) SEM photos of the PI, PU, and FEP surfaces, respectively, with a white scale bar of 5 μm. The film device is soft enough to bend or be attached to an irregular surface. (c) Schematic diagram of the sliding recognition by the single-electrode TENG. The object contacts with the FEP on the surface, which generates opposite charges on the two surfaces. (d) Schematic diagram of the capacitive part with an air gap encapsulated.

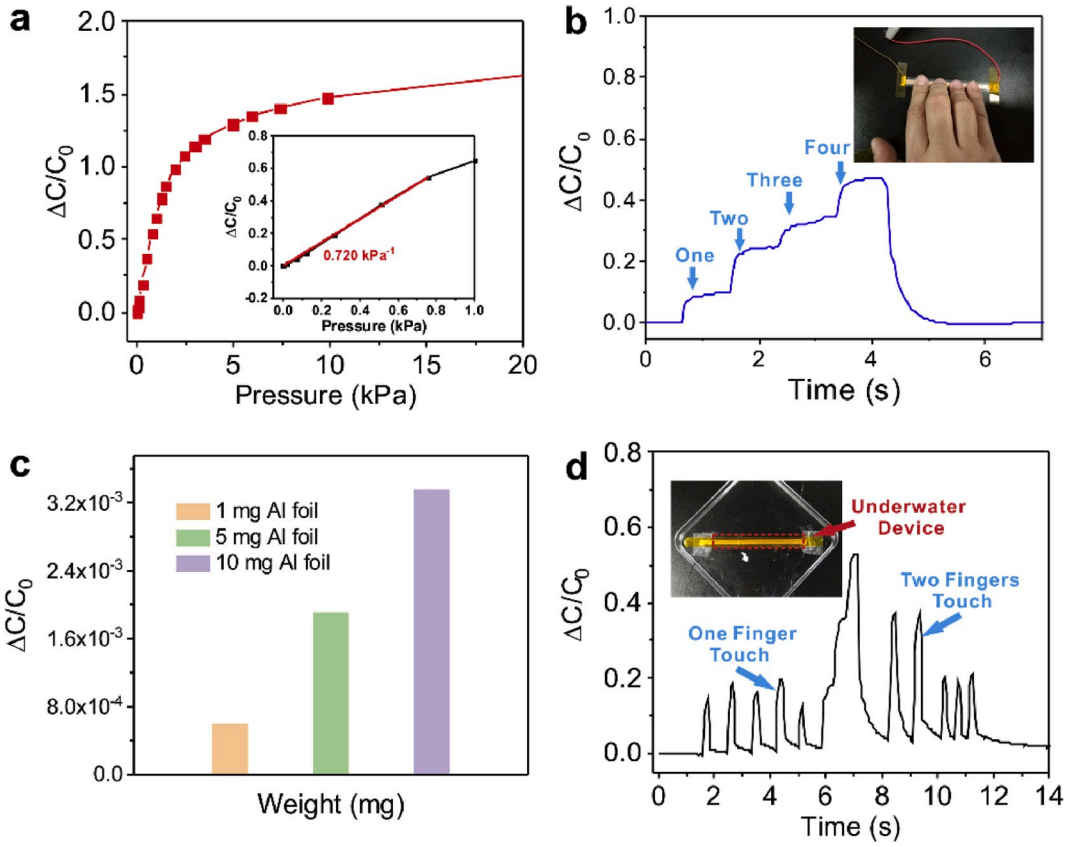

Fig. 2. Capacitive performance for the pressure of the flexible sliding sensor. (a) The ratio of the capacitive change to the vertical pressure curve was obtained by increasing the load on the flexible sliding sensor. (b) Four fingers were pressed on the device in the time sequence to verify the uniformity along the length direction. (c) The results of the small pressure test for the flexible sliding sensor, using 1 mg, 5 mg, and 10 mg Al foils. (d) The flexible sliding sensor could work underwater. The device was immersed in water and pressed by fingers.

the overlapping area dividing width. There were four capacitance platforms in accord with the four fingers touch in turn, shown in Fig. 2b. When the force was removed, the capacitance recovered to the original level. The results show that any pressure that occurs at the effective area could affect the shape of the air gap. We also compared the structure of one with the air gap and the other flatly sealed device on the capacitive performance (Fig. S3).

The response to small pressure is also tested for the device. Three

pieces of aluminum foil, weighing 1 mg, 5 mg and 10 mg respectively, are selected as samples. The average thickness of the aluminum foil was 15 μm, in case the deformation of the air gap should be very effective on the capacitance change, so there is a small capacitance increase after placing the aluminum foil on the sliding sensor. In the experiment, the foil is transferred with a metal tweezer and placed gently on the surface of the device. The entire process was monitored by an LCR meter in real-time (Fig. S4). The capacitance bounces up due to the pressure and recovers to initial values after blowing away the aluminum foil. Three different samples could be identified with very low but distinguished pressure in Fig. 2c.

Also, the flexible sliding sensor is based on the adhesive layer-by-layer structure, and each film is tightly bonded to adjacent layers, which achieves basic waterproof properties. The sliding sensor with an effective length of 12 cm is fabricated for testing the underwater performance. The device was directly attached to the bottom of a square petri dish (side length 10 cm). Then, tap water was poured to submerge the device. In Fig. 2d, the device could still work underwater, and the uniformity remained good along the length direction (Video S1).

Supplementary video related to this article can be found at https://doi.org/10.1016/j.nanoen.2020.104764

To analyze the sensing deformation response, large deformation of the device is tested under increasing strains. As shown in Fig. 3a, the device is adjusted horizontally with two ends fixed at a linear motor and a three-dimensional displacement stage. In the experiment, a step-by-step displacement test imposes deformation on the sliding sensor. The deformation process is described in the schematic illustration of Fig. 3b. When the fixed ends approached each other, the PET film at the bottom arches to release the strains, and the slim device shows a good curvature at the beginning, as shown in Fig. 3a. The results in Fig. 3c partly illustrates the deformation effect on the capacitance performance. The sensitivity at the initial stage is larger, indicating that the compressive force is effective in this condition. However, as the distance further decreased, the fixed force at two ends is insufficient to compress the device further and the change of capacitance slowed down.

Furthermore, we study the influence of bending orientation on the device performance under deformation. The device is tested under convex and concave deformations respectively in Fig. 3d and e. There is a difference in internal stress, and the ratio of capacitance change is different under the same bending degree. Fig. 3f shows that the inconsistent deformation of two layers compresses the intermediate dielectric part. And the internal strains are responsible for the performance under convex and concave deformations. And the long cycling test in Fig. 3d and e demonstrate the stability of the sensor, until the breakage of the Cu tape. The results illustrate that the flexible sensor is more suitable on fingers to monitor bending, because inwards bending can induce a concave deformation of the device [37].

In the device, TENG is designed for contact electrification and induce potential difference under the triboelectric cover material. The mechanism of TENG makes it possible to sense the contact-sliding motion of the contact object, as long as the surface is charged and can attract opposite charges in the back electrode. The relative motion of the charged surface could transfer mechanical energy into electrical signals through the electrode.

The preparation of sensing displacement is in the Experimental Section. A small sheet of A4 paper is regarded as the sample and placed at a fixed start point to process initial contact. The linear motor pushes the sample forward. The results in Fig. 4a and b shows that the open-

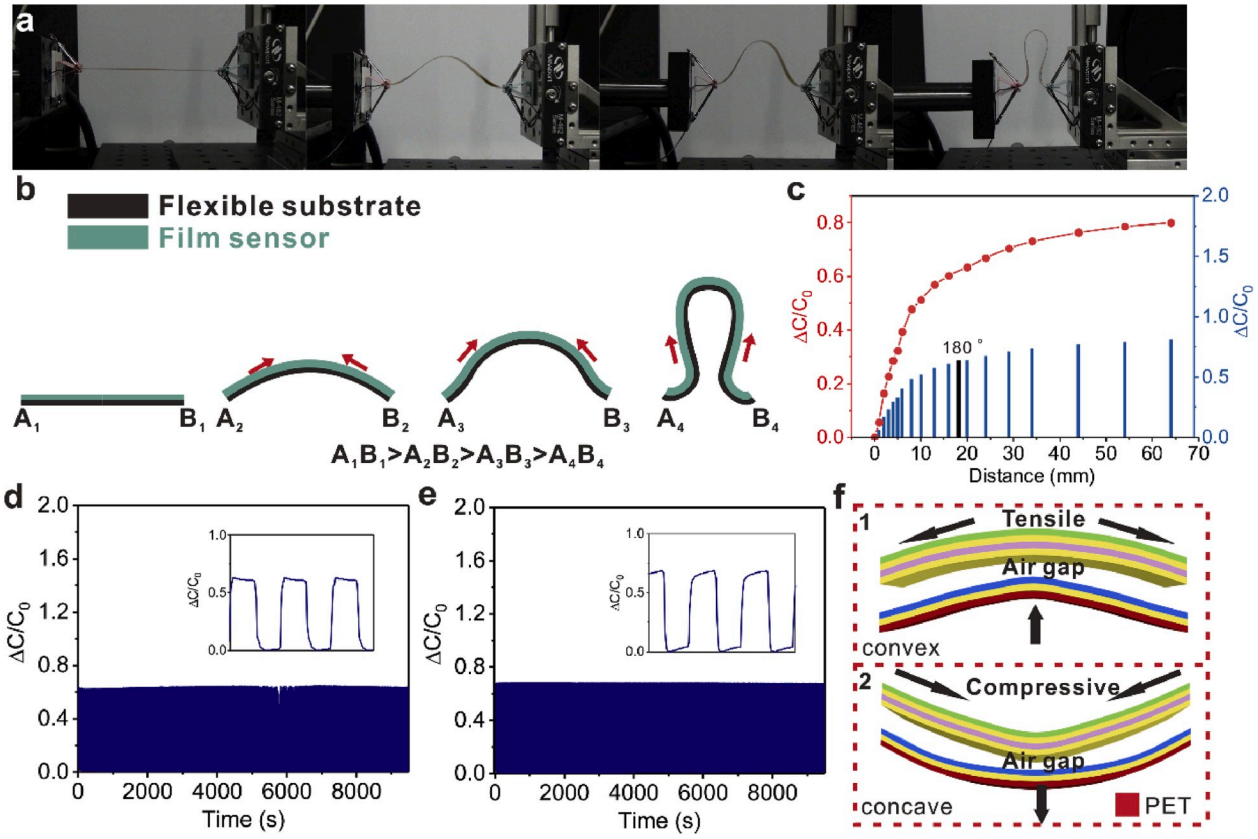

Fig. 3. Capacitive performance for the deformation of the flexible sliding sensor. (a) Photos of the striking process of the bending flexible sliding sensor. (b) Illustration of the deformation of the device due to the approaching distance and external force at the two fixed ends. (c) The effect of the deformation on the capacitive performance as the distance decreased. The 180° is an estimated bending angle for this measurement. (d) and (e) The cycling performance test of the flexible sliding sensor, for (d) upward convex and (e) downward concave deformations under the same striking process except for the orientation. (f) A schematic illustration of the convex and concave deformations, which were inconsistent in strain.

circuit voltage and transfer charges follow a linear relationship with the sliding displacement. The sensitivity to displacement is 0.1614 V m^{-1} and 53.92 nC m^{-1} for an 8 × 1 cm^2 flexible sliding sensor, and the contact area against the sample is kept as 1 × 1 cm^2. And the results were close to the report in the article based on the free-standing mode [38]. Then increasing velocity sensing test is carried out at a fixed displacement of 30 mm. The results in Fig. 4c show that the voltage holds on below the driving velocity of 0.2 ms^{-1}, then there is a drop in the signal. The voltage has a slight downtrend due to mechanical disturbances, which may come from the larger driving force and break the contact balance between solid films. Even though when the linear motor works stably, the voltage signals maintain. According to the results above, the TENG part could sense the sliding displacement of the contact object based on the open-circuit voltage and the number of transferred charges. The real-time signals generated from the sliding sensor are shown in Video S2.

Supplementary video related to this article can be found at https://doi.org/10.1016/j.nanoen.2020.104764

After further consideration of the transfer charges, the velocity could influence the number of charges through the circuit per second. This process is similar to change the working frequency of TENG to increase the height of current peaks [39]. In the experiment, the velocity gradually increases from 0.05 to 0.3 ms^{-1}, and short-circuit current is monitored under different sliding velocities. The results in Fig. 4d show that the average current peaks grow, which are distinguished for several cycles above the zero level. The sublevel part of the signals results from the backward motion at a velocity of 0.1 ms^{-1}. The current direction can reflect the forward and backward motions. In other words, a one-way movement toward the ground terminal of the device leads to a positive peak and then a negative peak in turn.

Displacement and velocity sensing results are tested by keeping the object contacting within the area of the triboelectric film and sliding on it. The contact electrification between the external object and the FEP film generate opposite charges on both surfaces, which is important to the device performance based on TENG (Fig. S5). But in this part the mechanism is a little different from the single-electrode mode or contact-sliding mode [40], because the previous two working modes require separation motion from contact. The non-separation process induces a small charge transfer in Fig. 4e. In the initial contact electrification, the sample and the FEP film carried an equal amount of charges, shown in Fig. 4e1. The charged sample on the surface changes the potential in the electrode and negative charges show the gradual change of potential in the electrode. During the process from Fig. 4e1 to Fig. 4e3, as the charged sample approaches the ground terminal, the potential around the resistor R gradually changes. The entire process is accompanied by a small amount of charge transfer. To demonstrate that surface charges generate the signals, the distance of the sample away from the triboelectric layer is also studied. The results show that the signals rapidly decrease when the sample separated from the sensor, but the sliding motion could still change the potential distribution in the electrode, even when it is 5 mm away (Fig. S6). This could be attributed to the surface charges which generate electrostatic field [41]. The mechanism reveals that displacement affects the number of transferred charges, and the current is related to the mechanical sliding velocity, which both constitutes the motion sensing function of the device to contact the object.

The flexible sliding sensor with an effective working length of 8 cm is prepared, and it is attached directly to the index finger that extended from tip to palm along the midline, as shown in Fig. 5a. In this condition, the sensor is soft enough to fit the epidermis tightly, and the epidermis could work both as a supporting substrate and an electrode for the capacitive part to monitor the finger bending and holding. Five steps of bending action and corresponding capacitance stages are recorded in Fig. 5b. When the finger releases, the capacitance could recover to the initial level. On the other hand, the attached device is directly used to recognize contact sliding. Different friction layers are used to

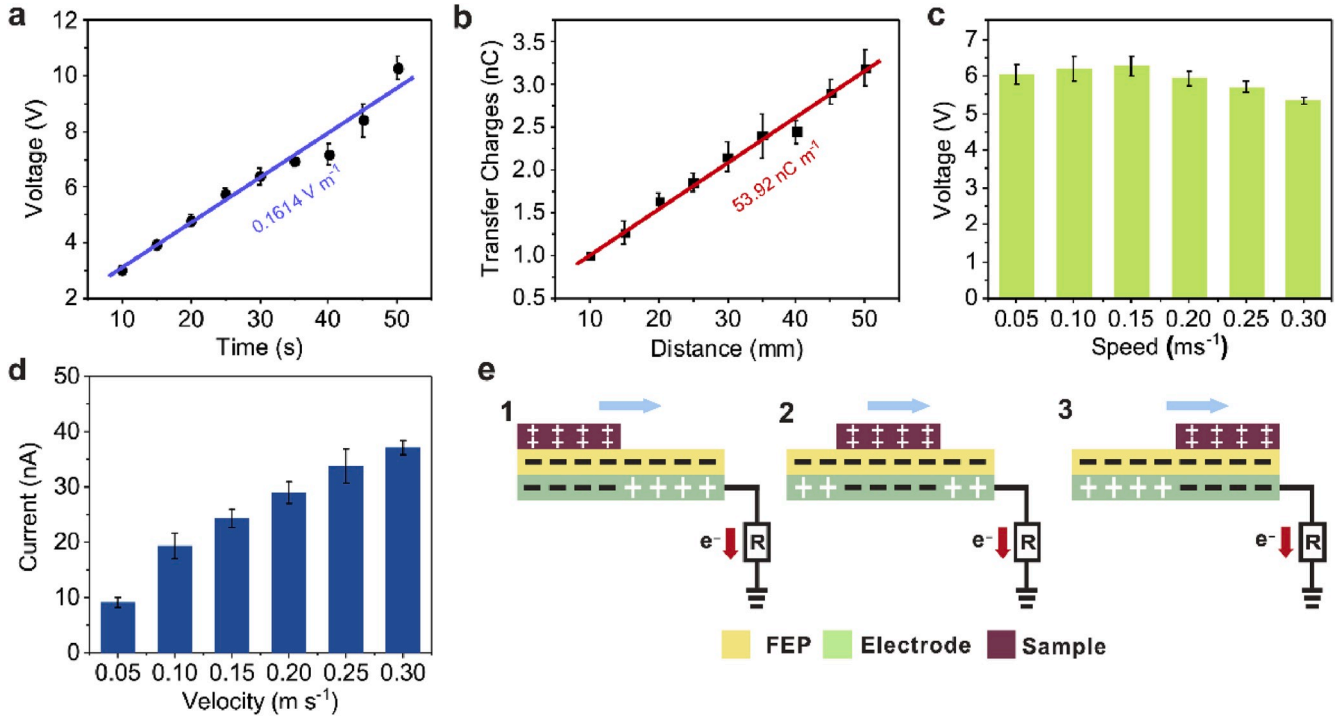

Fig. 4. Sensing the sliding displacement and velocity of the contact object with the corresponding output signals. (a) and (b) The open-circuit voltage (a) and the amount of transferred charge (b) were tested in the experiment at a fixed speed of 0.1 ms^{-1} for different displacements. (c) The test for a 30 mm displacement sliding, with velocity increasing from 0.05 to 0.3 ms^{-1}, to distinguish the effect of velocity from displacement. (d) The short-circuit current signal was tested from 0.05 to 0.3 ms^{-1} at a 30 mm displacement to show the influence of velocity on the current signal. (e) The working principle of the flexible sliding sensor in recognizing the sliding displacement and velocity of the contact object.

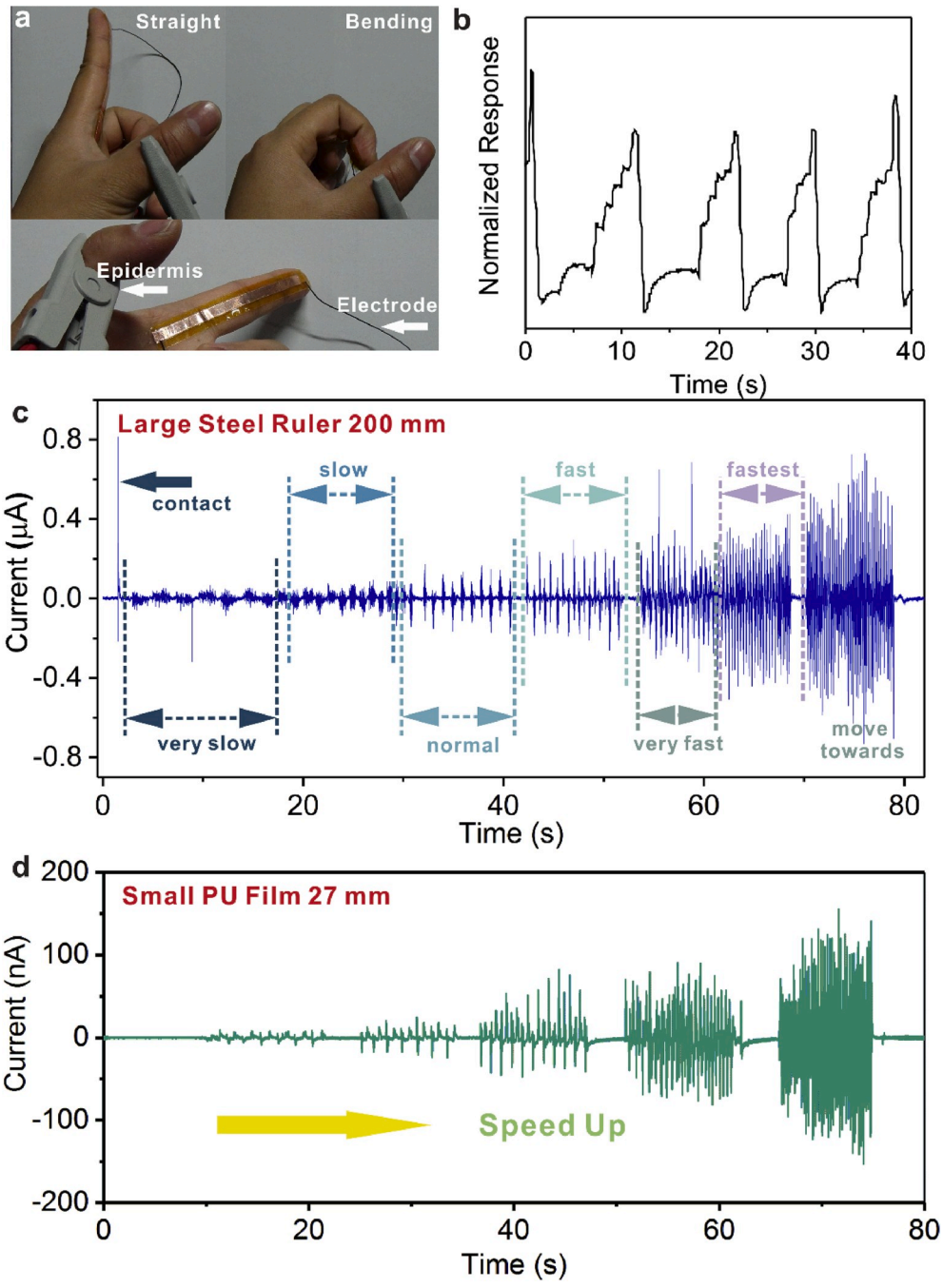

Fig. 5. The flexible sliding sensor is attached to the finger for bending and sliding sensing. (a) Photos of the device attached to the finger during the bending test. (b) The capacitance stages related to the five finger bending stages. (c) Current signals induced by the sliding of the steel ruler under increasing velocity. The ruler was 200 mm long. (d) Current signals induced by the sliding of the PU film under an increasing velocity. The PU film was 27 mm wide and smaller than the size of the sensor.

demonstrate that the sliding sensor works with contact objects. And the results in Fig. 5c and d are carried out to extend its application of handing driving Fig. 4d is a machine-driven result, and the velocity is controlled by a stable linear motor. And Fig. 5c and d are tested by sticking the sensor to a figure to fetch objects. Fig. 5c is a result of common contact-sliding TENG motion, which means the friction layer moves out of the device surface. In contrast, the result in Fig. 5d shows the non-separation process that the friction layer slides inside the area of the sensor. A stainless-steel ruler is used as a sample. There is a large and sharp current peak when the device first contacts the steel ruler. After that, the steel ruler slides back and forth by external force with long sides in parallel, and the corresponding signal is recorded in Fig. 5c for increasing velocity. The working mechanism of the flexible sliding sensor to detect the ruler motion in this condition is illustrated as contact-sliding mode TENG in Fig. S7. The current signal is also tested with a sheet of small PU film under increasing velocity. Compared to the large size of the steel ruler, the PU film is smaller than the area of the sliding sensor, so it follows the working mechanism shown in Fig. 4e. Overall, the current changes obviously to the velocity.

When trying to grip with the flexible sliding sensor, the device needs to be attached to the index finger to sense the process of gripping a 200 mL glass beaker, as shown in Fig. 6a. Firstly, we try to grip the beaker to test the capacitive part. When the hand seizes the beaker, the sensor closely contacts the outer wall of the beaker with triboelectric part outwards and capacitive part inside, and collects the information of finger bending and holding force to grip the beaker. So the effect on the capacitance is a combination of deformation and pressure. The results in Fig. 6b show three different gripping modes. Mode one is an attempt to seize the beaker in a short time, regardless of the gripping force. The capacitance remains high but drops suddenly when the force releases. In

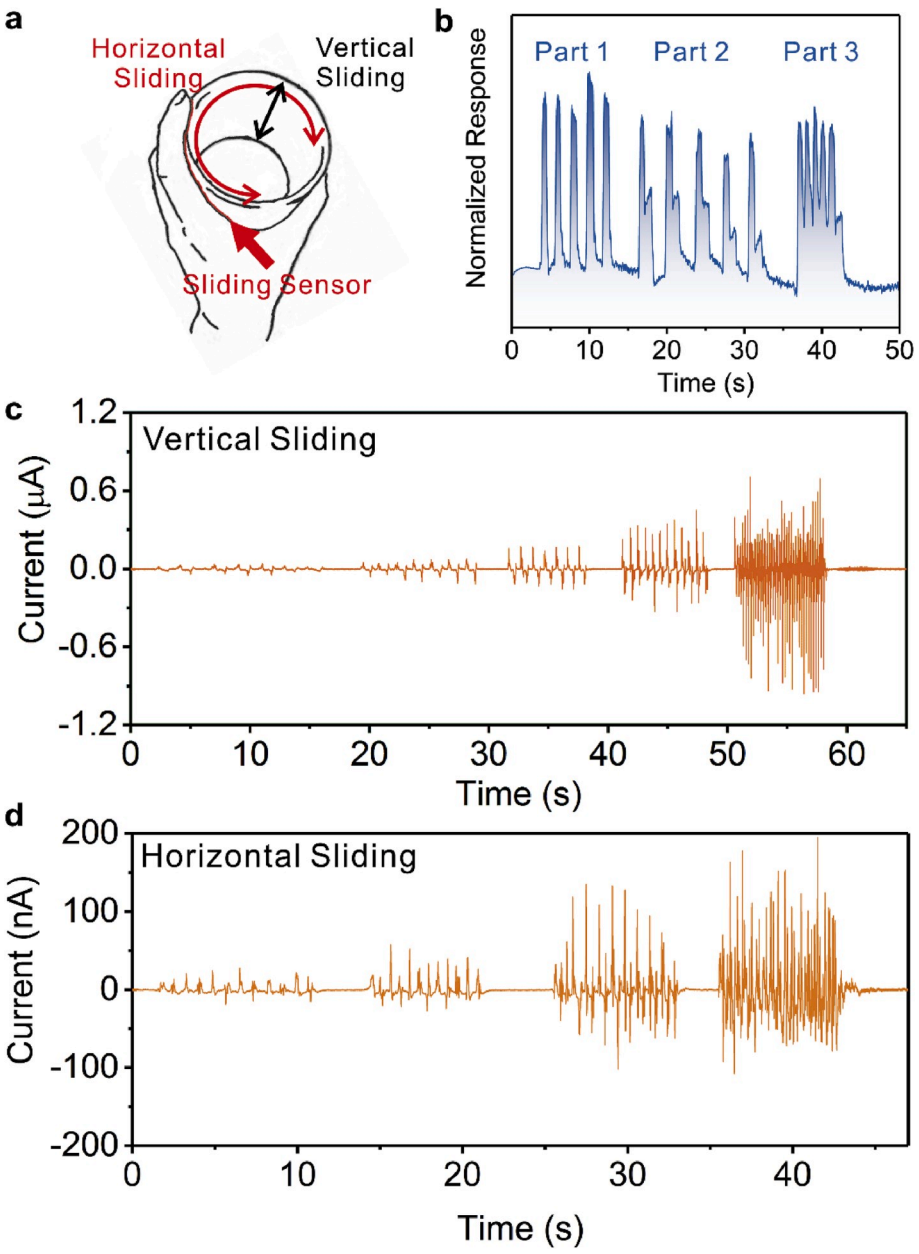

Fig. 6. Results of the hand-based sliding sensor to grip the beaker. (a) A schematic diagram of the test. The device was attached to the inside of the index finger to directly contact the beaker and to sense the sliding motion. (b) Gripping the beaker caused capacitive changes. Seizing and releasing the beaker (mode 1), holding the beaker and maintaining the gesture (mode 2), and the difference in the gripping force for holding (mode 3). (c) and (d) The triboelectric current signals induced by the vertical (c) and horizontal (d) sliding when gripping. The sliding velocity and direction impacted the current peaks.

mode two, the hand at first holds the beaker as in mode one, and then loses force while keeping bending. According to the results, capacitance drops by about half and recovers to the original level when finger unbent. Mode three reflects the different gripping force to hold. When the hand holds tightly and slightly, the capacitance changes with the gripping force.

The capacitive part senses the gripping and holding. However, while the robotic hand holds the object, it is often influenced by mechanical acceleration and vibration, which causes relative sliding. Compared to capacitive sensing, the sliding recognition based on the TENG sensor is a dynamic process [28]. We have studied that horizontal sliding from a small sheet of sample triggers regular signals of the flexible sliding sensor in Fig. 4. But the experiment for holding a larger beaker is in Fig. 6c and d. The triboelectric signals are induced by vertical and horizontal displacements, respectively. The vertical signals are larger than the horizontal ones due to the larger change of contact area in a short time. In addition, the forward and backward motions induce corresponding current peaks and the signals increase with sliding velocity while the object is gripped.

4. Conclusion

A multifunctional, thin and flexible sliding sensor that combines a capacitive sensor with a TENG based sensor to detect compressive pressure, deformation and displacement, the velocity of contact objects have been developed. This device is designed for flexible robotic manipulators to achieve high sensitivity and intelligent recognition of gripping force. The combination of the two sensing parts can realize the conversion of the physical signals to the electrical ones in the soft gripping process, and finally realize the functions of the sliding sensor.

The whole device is based on a layer-by-layer structure that is convenient for packaging to work underwater. The introduction of the air gap as the dielectric layer in the device significantly increases the sensitivity to pressure, especially in the slight region. On the other hand, the TENG part can sense the sliding motion and achieves a linear relationship between the displacement of contact objects and detected transfer charges. Furthermore, the peaks of current signals can reflect the sliding velocity of the contact object. Above all, the flexible sliding sensor can collect the information of gripping an object, which is

attributed to judging the conditions and adjusting the force for the robotic arm. We could extend our approach to fingers and robotic arms to grip fragile and soft objects. The sliding sensor can be part of the tactile sensing system for robotic hands.

Declaration of competing interest

The authors declare that they have no known competing financial interests or personal relationships that could have appeared to influence the work reported in this paper.

CRediT authorship contribution statement

Zuqing Yuan: Writing - original draft, Writing - review & editing, Investigation, Formal analysis, Methodology, Software. **Guozhen Shen:** Project administration, Resources, Supervision, Validation, Funding acquisition. **Caofeng Pan:** Project administration, Resources, Supervision, Validation, Funding acquisition. **Zhong Lin Wang:** Project administration, Resources, Supervision, Validation, Funding acquisition.

Acknowledgements

The authors thank the support of the national key R & D project from the Minister of Science and Technology, China (2016YFA0202703 and 2016YFA0202704), the National Natural Science Foundation of China (No. 51622205, 61675027, 51432005, 61505010 and 51502018), the Beijing City Committee of science and technology (Z171100002017019 and Z181100004418004), the Natural Science Foundation of Beijing Municipality (4181004, 4182080, 4184110, 2184131 and Z180011), and the University of Chinese Academy of Sciences.

Appendix A. Supplementary data

Supplementary data to this article can be found online at https://doi.org/10.1016/j.nanoen.2020.104764.

References

[1] T. Okada, IEEE T. Syst. Man. Cy-S. 12 (1982) 289–299.
[2] M.T. Mason, IEEE T. Syst. Man. Cy-S. 11 (1981) 418–432.
[3] L.R. Hochberg, D. Bacher, B. Jarosiewicz, N.Y. Masse, J.D. Simeral, J. Vogel, S. Haddadin, J. Liu, S.S. Cash, P. Van Der Smagt, Nature 485 (2012) 372–375.
[4] G. Palli, C. Natale, C. May, C. Melchiorri, T. Wurtz, IEEE-ASME T. Mech. 18 (2012) 664–673.
[5] C. Li, T. Zhang, D.I. Goldman, Science 339 (2013) 1408–1412.
[6] E. Kizilkan, J. Strueben, A. Staubitz, S.N. Gorb, Sci. Robot. 2 (2017).
[7] S.A. Morin, R.F. Shepherd, S.W. Kwok, A.A. Stokes, A. Nemiroski, G.M. Whitesides, Science 337 (2012) 828–832.
[8] D. Rus, M.T. Tolley, Nature 521 (2015) 467–475.
[9] M.A. Graule, P. Chirarattananon, S.B. Fuller, N.T. Jafferis, K.Y. Ma, M. Spenko, R. Kornbluh, R.J. Wood, Science 352 (2016) 978–982.
[10] P. Rothemund, A. Ainla, L. Belding, D.J. Preston, S. Kurihara, Z. Suo, G. M. Whitesides, Sci. Robot. 3 (2018) eaar7986.
[11] D.P.J. Cotton, P.H. Chappell, A. Cranny, N.M. White, S.P. Beeby, IEEE Sensor. J. 7 (2007) 752–761.
[12] S. Sundaram, P. Kellnhofer, Y. Li, J.-Y. Zhu, A. Torralba, W. Matusik, Nature 569 (2019) 698–702.
[13] M.T. Francomano, D. Accoto, E. Guglielmelli, IEEE Sensor. J. 13 (2013) 2489–2498.
[14] Z. Kappassov, J.-A. Corrales, V. Perdereau, Robot. Autonom. Syst. 74 (2015) 195–220.
[15] X. Lai, K. Cao, G. Shen, P. Xue, D. Wang, F. Hu, J. Zhang, Q. Yang, X. Wang, Sci. Bull. 63 (2018) 187–193.
[16] X. Wang, D. Peng, B. Huang, C. Pan, Z.L. Wang, Nano Energy 55 (2019) 389–400.
[17] M. Tang, P. Xu, Z. Wen, X. Chen, C. Pang, X. Xu, C. Meng, X. Liu, H. Tian, N. Raghavan, Sci. Bull. 63 (2018) 1118–1124.
[18] C. Wang, J. Zhao, C. Ma, J. Sun, L. Tian, X. Li, F. Li, X. Han, C. Liu, C. Shen, Nano Energy 34 (2017) 578–585.
[19] C. Pan, M. Chen, R. Yu, Q. Yang, Y. Hu, Y. Zhang, Z.L. Wang, Adv. Mater. 28 (2016) 1535–1552.
[20] S. Qiao, J. Liu, G. Fu, K. Ren, Z. Li, S. Wang, C. Pan, Nano Energy 49 (2018) 508–514.
[21] L. Wang, S. Chen, W. Li, K. Wang, Z. Lou, G. Shen, Adv. Mater. 31 (2019) 1804583.
[22] H. Khamis, R.I. Albero, M. Salerno, A.S. Idil, A. Loizou, S.J. Redmond, Sensor Actuat. A-Phys. 270 (2018) 195–204.
[23] N. Morita, H. Nogami, E. Higurashi, R. Sawada, Sensors 18 (2018) 326.
[24] Z. Lei, Q. Wang, S. Sun, W. Zhu, P. Wu, Adv. Mater. 29 (2017) 1700321.
[25] M.S. Sarwar, Y. Dobashi, C. Preston, J.K.M. Wyss, S. Mirabbasi, J.D.W. Madden, Sci. Adv. 3 (2017), e1602200.
[26] Z.L. Wang, ACS Nano 7 (2013) 9533–9557.
[27] Q. Shen, X. Xie, M. Peng, N. Sun, H. Shao, H. Zheng, Z. Wen, X. Sun, Adv. Funct. Mater. 28 (2018) 1703420.
[28] X. Xie, Z. Wen, Q. Shen, C. Chen, M. Peng, Y. Yang, N. Sun, P. Cheng, H. Shao, Y. Zhang, Adv. Mater. Technol. 3 (2018) 1800054.
[29] X. Xie, Y. Zhang, C. Chen, X. Chen, T. Yao, M. Peng, X. Chen, B. Nie, Z. Wen, X. Sun, Nano Energy 65 (2019) 103984.
[30] H. Qin, G. Gu, W. Shang, H. Luo, W. Zhang, P. Cui, B. Zhang, J. Guo, G. Cheng, Z. Du, Nano Energy 68 (2020) 104372.
[31] F. Yang, J. Guo, L. Zhao, W. Shang, Y. Gao, S. Zhang, G. Gu, B. Zhang, P. Cui, G. Cheng, Nano Energy 67 (2020) 104210.
[32] H. Qin, G. Cheng, Y. Zi, G. Gu, B. Zhang, W. Shang, F. Yang, J. Yang, Z. Du, Z. L. Wang, Adv. Funct. Mater. 28 (2018) 1805216.
[33] Y. Yang, H. Zhang, J. Chen, Q. Jing, Y.S. Zhou, X. Wen, Z.L. Wang, ACS Nano 7 (2013) 7342–7351.
[34] Z.L. Wang, Mater. Today 20 (2017) 74–82.
[35] H. Zou, Y. Zhang, L. Guo, P. Wang, X. He, G. Dai, H. Zheng, C. Chen, A.C. Wang, C. Xu, Nat. Commun. 10 (2019) 1–9.
[36] S.C.B. Mannsfeld, B.C.K. Tee, R.M. Stoltenberg, C.V.H.H. Chen, S. Barman, B.V. O. Muir, A.N. Sokolov, C. Reese, Z. Bao, Nat. Mater. 9 (2010) 859–864.
[37] L. Dhakar, P. Pitchappa, F.E.H. Tay, C. Lee, Nano Energy 19 (2016) 532–540.
[38] Q. Jing, Y. Xie, G. Zhu, R.P.S. Han, Z.L. Wang, Nat. Commun. 6 (2015) 8031.
[39] G. Zhu, J. Chen, T. Zhang, Q. Jing, Z.L. Wang, Nat. Commun. 5 (2014) 3426.
[40] W. Ding, A.C. Wang, C. Wu, H. Guo, Z.L. Wang, Adv. Mater. Technol. 4 (2019) 1800487.
[41] J. Wang, C. Wu, Y. Dai, Z. Zhao, A. Wang, T. Zhang, Z.L. Wang, Nat. Commun. 8 (2017) 1–8.

Zuqing Yuan received his B.S. degree from the Department of Materials Science and Engineering from University of Science and Technology Beijing (USTB) in 2014. And then he earned his Ph.D.degree from Beijing Institute of Nanoenergy and Nanosystems, Chinese Academy of Sciences in 2019. His main research interests focus on the nanomaterials, polymer-based energy harvesting and smart device for flexible electronics.

Prof. Guozhen Shen received his B. S. degree (1999) in Chemistry from Anhui Normal University and Ph. D degree (2003) in Chemistry from University of Science and technology of China. Before joining Institute of Semiconductors, Chinese Academy of Sciences, he worked in Hanyang University (Korea), National Institute for Materials Science (Japan), University of Southern California (US), and Huazhong University of Science and Technology (China). His current research focused on developing flexible electronic devices for artificial intelligence and healthcare monitoring.

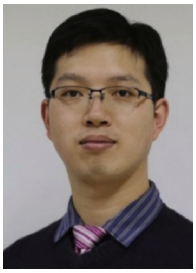

Prof. Caofeng Pan received his B.S. degree (2005) and his Ph. D. (2010) in Materials Science and Engineering from Tsinghua University, China. He then joined the Georgia Institute of Technology as a postdoctoral fellow. He is currently a professor and a group leader at Beijing Institute of Nanoenergy and Nanosystems, Chinese Academy of Sciences since 2013. His main research interests focus on the felds of piezotronics/piezophototronics for fabricating new electronic and optoelectronic devices, and self-powered nanosystems. Details can be found at http://www.piezotronics.cn.

Prof. Zhong Lin (ZL) Wang received his Ph.D. from Arizona State University in physics. He now is the Hightower Chair in Materials Science and Engineering, Regents' Professor, Engineering Distinguished Professor and Director, Center for Nanostructure Characterization, at Georgia Tech. Dr. Wang has made original and innovative contributions to the synthesis, discovery, characterization and understanding of fundamental physical properties of oxide nanobelts and nanowires, as well as applications of nanowires in energy sciences, electronics, optoelectronics and biological science. His discovery and breakthroughs in developing nanogenerators established the principle and technological road map for harvesting mechanical energy from environment and biological systems for powering a personal electronics. His research on self-powered nanosystems has inspired the worldwide effort in academia and industry for studying energy for micro-nano-systems, which is now a distinct disciplinary in energy research and future sensor networks. He coined and pioneered the field of piezotronics and piezophototronics by introducing piezoelectric potential gated charge transport process in fabricating new electronic and optoelectronic devices. Details can be found at: http://www.nanoscience.gatech.edu.